A Bipolar Delayed Fluorescence Luminogen with Fast Reverse Intersystem Crossing and High Horizontal Dipole Orientation for High-Performance Sky-Blue and White OLEDs

Yan Fu, Hao Liu, Dezhi Yang, Dongge Ma, Zujin Zhao, and Ben Zhong Tang*

Y. Fu, H. Liu, Dr. D. Yang, Prof. D. Ma, Prof. Z. Zhao, Prof. B. Z. Tang
State Key Laboratory of Luminescent Materials and Devices, Guangdong Provincial Key Laboratory of Luminescence from Molecular Aggregates, South China University of Technology, Guangzhou 510640, China.
E-mail: mszjzhao@scut.edu.cn
Prof. B. Z. Tang
Shenzhen Institute of Aggregate Science and Technology, School of Science and Engineering, The Chinese University of Hong Kong, Shenzhen, Guangdong 518172, China.
Prof. B. Z. Tang
Hong Kong Branch of Chinese National Engineering Research Center for Tissue Restoration & Reconstruction, The Hong Kong University of Science and Technology, Clear Water Bay, Hong Kong, China.

Keywords: delayed fluorescence, reverse intersystem crossing, bipolar carrier transport, organic light-emitting diode, out-of-phase sensitizing

Abstract: The development of robust luminescent materials plays a key role for organic light-emitting diodes (OLEDs). Herein, a tailor-made sky-blue delayed fluorescence luminogen (DCPC-BP-SFAC) containing a carbonyl acceptor and spiro[acridine-9,9'-fluorene] and 9,9'-(cyclohexane-1,1-diylbis(4,1-phenylene))bis(9H-carbazole) donors is explored, which holds merits of excellent thermal stability, strong photoluminescence, balanced carrier transport and horizontal dipole orientation. Owing to a charge-transfer dominated singlet state and a charge-transfer and local-excitation hybrid triplet state, DCPC-BP-SFAC has a small energy gap between singlet and triplet as well as a large spin–orbit coupling constant, which result in a fast reverse intersystem crossing process and thus efficient delayed fluorescence. High-performance sky-blue OLEDs with outstanding external quantum efficiencies (η_{ext}s) reaching 32.6% are achieved based on DCPC-BP-SFAC, benefiting from high exciton utilization and large light-out coupling efficiency. Moreover, using DCPC-BP-SFAC as blue emitter and host material

simultaneously, efficient all-fluorescence out-of-phase sensitizing white OLEDs without inter-layer are fabricated, providing high η_{ext}s of up to 21.6% and stable warm-white light with a high color rendering index of 84. The outstanding electroluminescence performances demonstrate the great potentials of DCPC-BP-SFAC in practical display and lighting devices.

1. Introduction

Organic light-emitting diodes (OLEDs) have presented great potentials and merits in flat-panel display and white-light illumination, and continuously increasing efforts from both academic and industry have been devoted to improve the electroluminescence (EL) performances of the devices to meet the requirements for widespread commercialization.[1] The external quantum efficiency (η_{ext}), an important parameter for evaluating OLED performance, is determined by exciton utilization efficiency (η_r), carrier balance factor (γ), photoluminescence (PL) quantum yield (Φ_{PL}) and light out-coupling efficiency (η_{out}).[2] From conventional fluorescence materials to phosphorescence and thermally activated delayed fluorescence (TADF) materials, the theoretical boundary of η_r has increased from 25% to 100%, achieving the full utilization of 75% triplet excitons through intersystem crossing (ISC) or reverse intersystem crossing (RISC) processes.[3] However, the conversion between singlet and triplet excitons is a process involving the spin flip of electron. The phosphorescence materials containing heavy metal elements can undergo this process by heavy atom effect, but these noble metals such as iridium and platinum are actually expensive.[4] As for purely organic TADF emitters, small singlet and triplet energy splitting (ΔE_{ST}) values and large spin–orbit coupling (SOC) constants are essential for efficient RISC process.[5] Generally, small ΔE_{ST} values can be achieved by constructing a twisted electronic donor-acceptor (D-A) structure, and large SOC values can be acquired by different transition types of singlet and triplet states, which is favoured to the change of angular momentum.

Recently, the vigorous developments of TADF materials have brought about more and more efficient luminescent materials with excellent EL performance.[6] Among them, a small

portion of TADF materials can be used not only as emitters but also as host materials, providing new perspectives for the exploration of host materials.[7] Owing to the large energy gaps of traditional host materials, excitons generally recombine on guest materials rather than the host materials, which may lead to serious exciton-polaron annihilation at high voltages.[8] For the host materials from TADF emitters, excitons can directly form on them, and then transfer to the guests through Förster energy transfer (FET) and Dexter energy transfer (DET). Since these processes involve triplet excitons, the mitigation of triplet-triplet annihilation (TTA) should be considered in molecular design. In view of this, the TADF emitters that have excellent EL performances in neat films are of high potentials for the use as host materials as well, which is conducive to simplifying manufacturing process, broadening exciton recombination zone and improving device repeatability.[9,7a,7c]

In this work, a novel sky-blue luminogen (DCPC-BP-SFAC) composed by electron-donors spiro[acridine-9,9'-fluorene] (SFAC) and 9,9'-(cyclohexane-1,1-diylbis(4,1-phenylene))bis(9H-carbazole) (DCPC) and an electron-acceptor carbonyl (BP) is designed and synthesized. SFAC and BP are in charge of building a twisted D-A type configuration responsible for the generation of delayed fluorescence. And the presence of SFAC is also beneficial for increasing horizontal dipole ratio ($\Theta_{//}$) of the molecule, which is an effective program to improve η_{out}.[10] DCPC is employed to enhance bipolar property and balance carrier mobility.[11] Meanwhile, the bulky functional groups of DCPC and SFAC can also increase the intermolecular distance, thus weakening the interaction between adjacent luminogenic molecules and alleviating emission quenching in solid state. Notably, the transition characteristic of the lowest triplet excited (T_1) state involves both local-excitation (LE) and charge-transfer (CT), while the lowest singlet excited (S_1) state is dominated by the CT-type transition, which lead to a small ΔE_{ST} and a large SOC at the same time. Because of these outstanding properties, DCPC-BP-SFAC performs efficiently in sky-blue OLEDs with remarkable η_{ext} values of up to 32.6%. Moreover, high-performance all-fluorescence white OLEDs (WOLEDs) are achieved using

DCPC-BP-SFAC as both blue emitter and host material, providing stable warm-white light and brilliant EL efficiencies.

2. Results and Discussion

2.1. Synthesis and Characterization

2.1.1. Synthesis

DCPC-BP-SFAC is synthesized using the Friedel-Crafts acylation and Buchwald-Hartwig cross coupling reaction, and the detailed synthetic route is depicted in Scheme 1. The preparation procedures and characterization data of NMR and high-resolution mass spectrometry are described in Supporting Information. DCPC-BP-SFAC is isolated with column chromatography and further purified by sublimation before photophysical property measurement and application in OLEDs. It has good solubility in common organic solvents such tetrahydrofuran (THF), dichloromethane, chloroform and toluene, but is hardly soluble in water and methanol.

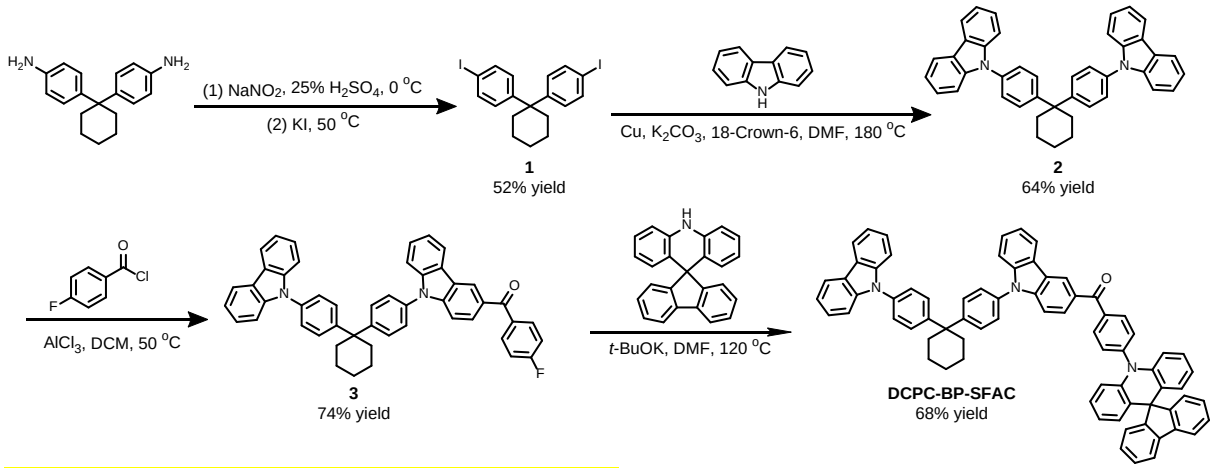

Scheme 1. Synthetic route of DCPC-BP-SFAC.

2.1.2. Thermal Stability and Electrochemical Behavior

The thermal stability of DCPC-BP-SFAC is examined by thermogravimetric analysis (TGA) and differential scanning calorimetry (DSC). As shown in **Figure 1**A, DCPC-BP-SFAC possesses excellent thermal and morphological stabilities. The decomposition temperature (T_d, at 5% loss of initial weight) and the glass-transition temperature (T_g) are as high as 521 and 199 °C, respectively, which are sufficient for the application in vacuum-deposited OLEDs. The

electrochemical stability is evaluated by cyclic voltammetry (Figure 1B). DCPC-BP-SFAC shows reversible oxidation and reduction processes, indicating its good electrochemical stability. The initial oxidation and reduction potentials against Fc/Fc^+ redox couple are 0.55 and −2.12 V, respectively. Hence, the HOMO and LUMO energy levels are estimated to be −5.35 and −2.68 eV, which are applicable for carrier injection in OLEDs.

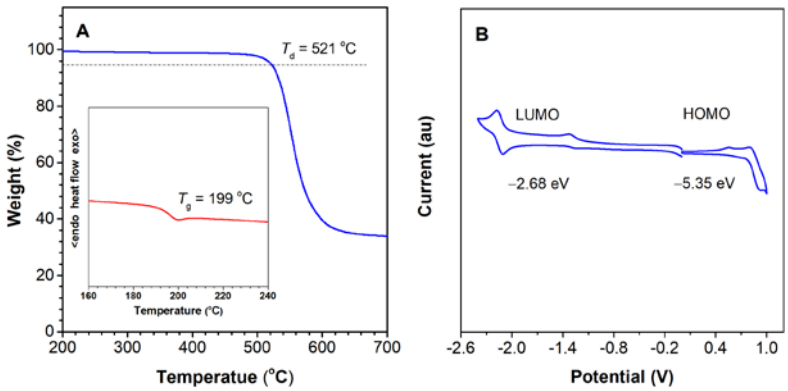

Figure 1. (A) TGA and DSC thermograms of DCPC-BP-SFAC. T_d is decomposition temperature, corresponding to 5% loss of initial weight. T_g is glass-transition temperature. (B) Cyclic voltammograms of DCPC-BP-SFAC, measured in dichloromethane (HOMO energy level) and dimethylformamide (LUMO energy level) containing 0.1 M tetra-*n*-butylammonium hexafluorophosphate.

2.1.3 Photophysical Properties

The ultraviolet-visible absorption and photoluminescence (PL) spectra of DCPC-BP-SFAC are measured in diluted toluene solution (10^{-5} M). As displayed in **Figure 2**A, DCPC-BP-SFAC shows an absorption maximum at 340 nm, associated with the π−π* transitions of the molecular backbone. A broad absorption tail extending to 440 nm is recorded, which is assigned to the intramolecular charge transfer (ICT) from SFAC donor to carbonyl acceptor. DCPC-BP-SFAC displays a sky-blue PL peak at 473 nm with a Φ_{PL} value of 48% in toluene. But in polar tetrahydrofuran (THF) solution, the PL peak is red-shifted to 503 nm with a decreased Φ_{PL} value of 7%, due to the strengthened ICT effect. By adding a small amount of poor solvent water to THF

solution, the PL peak is weakened and red-shifted to some degree, due to the enhanced ICT effect by the increased polarity of the THF/water mixture (Figure 2B).[12] But along with the increase of water fraction (f_w, vol%) in the mixture, the PL peak is enhanced greatly and blue-shifted. On the other hand, the PL decay curves in THF/water mixtures show that as the increase of f_w from 0 to 99 vol%, the PL lifetime rises substantially from 43.0 ns to 1239.3 ns, accompanied with increasingly apparent delayed fluorescence (Figure 2C). Since DCPC-BP-SFAC is insoluble in water, it forms nanoaggregates at a high f_w, and the polarity of the nanoaggregates is reduced in comparison with the THF/water mixture. In addition, the intramolecular motion is restricted by the spatial constraint in nanoaggregates and thus the nonradiative decay of the excited state is blocked. These factors result in enhanced and blue-shifted PL peak as well as the appearance of delayed fluorescence.[9a,9c,12]

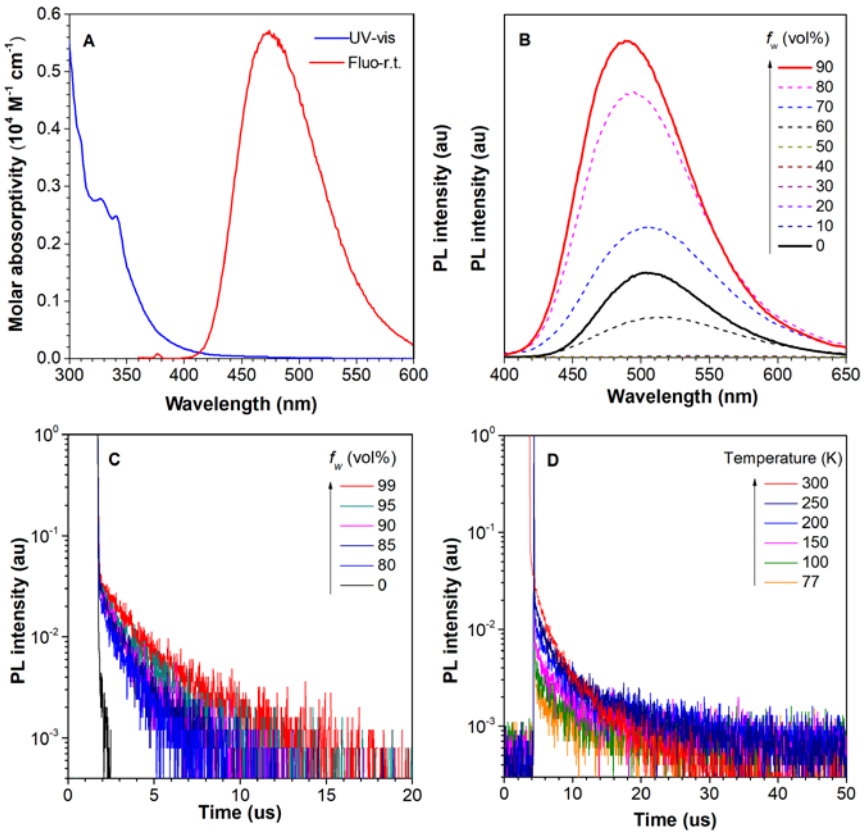

Figure 2. (A) Absorption and PL spectra of DCPC-BP-SFAC in diluted toluene solution. (B) PL spectra and (C) PL decay curves of DCPC-BP-SFAC in THF/water mixtures with different

water fractions (f_w). (D) Temperature-dependent PL decay curves of DCPC-BP-SFAC neat film, measured under nitrogen.

The photophysical properties of DCPC-BP-SFAC in neat and doped films are further studied. Herein, 2,8-bis(diphenylphosphoryl)dibenzo[b,d]furan (PPF) is chosen as the host on account of its high triplet energy level (3.0 eV),[13] and the doped film is fabricated at a doping concentration of 20 wt%. The PL spectra of the neat and doped films are similar, with close PL peaks at around 483 nm. The Φ_{PL} values of the neat film and doped film are recorded as 47% and 90%, respectively. Then, the fluorescence and phosphorescence spectra are measured at 77 K to obtain the ΔE_{ST} values (Figure S1). From the onsets of these spectra, the S_1 and T_1 energy levels are calculated to be 2.82 and 2.74 eV for the neat film, and 2.86 and 2.83 eV for the doped film. Hence, the corresponding ΔE_{ST} values are 0.084 and 0.037 eV for the neat and doped films, respectively, which are small enough for the occurrence of RISC progress from T_1 to S_1 states.

The transient PL behaviors of neat and doped films of DCPC-BP-SFAC are recorded under nitrogen atmosphere (Figure 2D and Figure S2C). The PL emissions of the neat and doped films decay in a double exponential model consisting of a nanosecond-scale component and a microsecond-scale one, which belong to prompt fluorescence and delayed fluorescence, respectively. The decay of PL emission is sensitive to temperature. By raising temperature from 77 to 300 K, the ratio of delayed component is significantly increased on account of the promoted RISC process at high temperatures, exhibiting a typical TADF characteristic. At 300 K, the lifetimes of delayed components of the neat and doped films are 4.5 and 6.1 μs, respectively. Based on the photophysical data (Table S1), the corresponding transition rate constant is estimated (Table S2).[14] Both neat and doped films have fast RISC processes with large rate constants (k_{RISC}) of 1.2×10^6 s^{-1} and 2.2×10^6 s^{-1}, respectively.

2.1.4. Horizontal Dipole Orientation

To study the orientation of the emitting dipole of DCPC-BP-SFAC, the angle-dependent *p*-polarized PL spectra of the neat and doped films are measured. As shown in **Figure 3**A and B, the $\Theta_{//}$ values of the neat and doped films reach up to 83% and 85%, respectively, indicating that DCPC-BP-SFAC tends to be anisotropic and aligned parallel to the substrate no matter in neat or doped films. This can be ascribed to the effect of SFAC that prolongs molecular length along the transition dipole moment (Figure 3C).[11a] The horizontal orientation for the emitting dipole of DCPC-BP-SFAC can afford high η_{out} values to improve the η_{ext} values for the OLEDs.

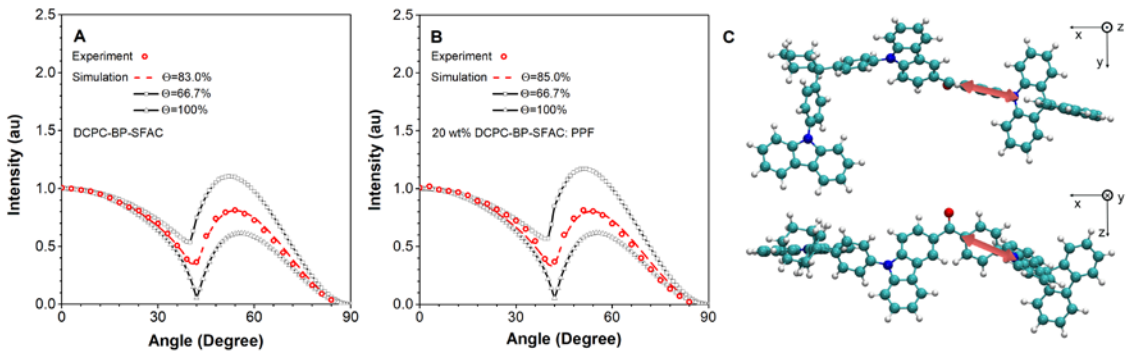

Figure 3. Measured horizontal transition dipole moment ratio of (A) the neat film and (B) the doped film of DCPC-BP-SFAC. (C) The direction of the transition dipole moment (as indicated by the red arrow) of DCPC-BP-SFAC relative to the coordinates of the molecular structure.

2.1.5. Theoretical Calculation and Analysis

The density functional theory (DFT) and time-dependent density functional theory (TDDFT) simulations are employed to gain deep insights into the geometrical and electronic structures of DCPC-BP-SFAC (**Figure 4**). According to the optimized molecular geometry in ground state (S_0), the acceptor and donor segments are connected in a highly twisted conformation with a large torsion angle of 84.7º. Similar to the configuration of S_0 state, the S_1 state also adopts a tortile configuration accompanied with a large torsion angle of 88.9º between SFAC and phenyl bridge. On the basis of the analysis of the natural transition orbital (NTO) of S_1 state, the highest occupied NTO (HONTO) and the lowest unoccupied NTO (LUNTO) are separated sufficiently

with the HONTO mainly focusing on the acridine segment of SFAC, and the LUNTO distributing on carbonyl core, phenyl bridge and part of carbazole group nearby the carbonyl. Such kind of NTO distribution reveals a charge-transfer (CT) characteristic, which benefits from the tortile configuration of S_1 state. It is worth noticing that the transition of T_1 state is not an absolute CT or local-excitation (LE) but a mixture of CT and LE. The LUNTO distribution of T_1 state is identical to that of S_1 state, but the HONTO distribution of T_1 state, which expands from SFAC donor to carbonyl acceptor with 52.28% located on the acceptor and 47.78% situated at donor, is much wider than that of S_1 state (Figure 4B). Meanwhile, the orbital overlap ratio is only 56% and the centroid distance between HONTO and LUNTO reaches 3.02 Å. Therefore, according to the electronic diagram and quantitative values, the transition of T_1 state is rationalized to be a hybrid characteristic of LE and CT. Particularly, for the HONTO, the orbital distributed on carbonyl acceptor exhibits a n-type feature, differing from that of the LUNTO (π^*-type), while the rest of the orbital has a π-type feature (Figure 4C). Hence, the transition characteristic of T_1 state combines the LE (n, π^*) and CT (π, π^*) together.

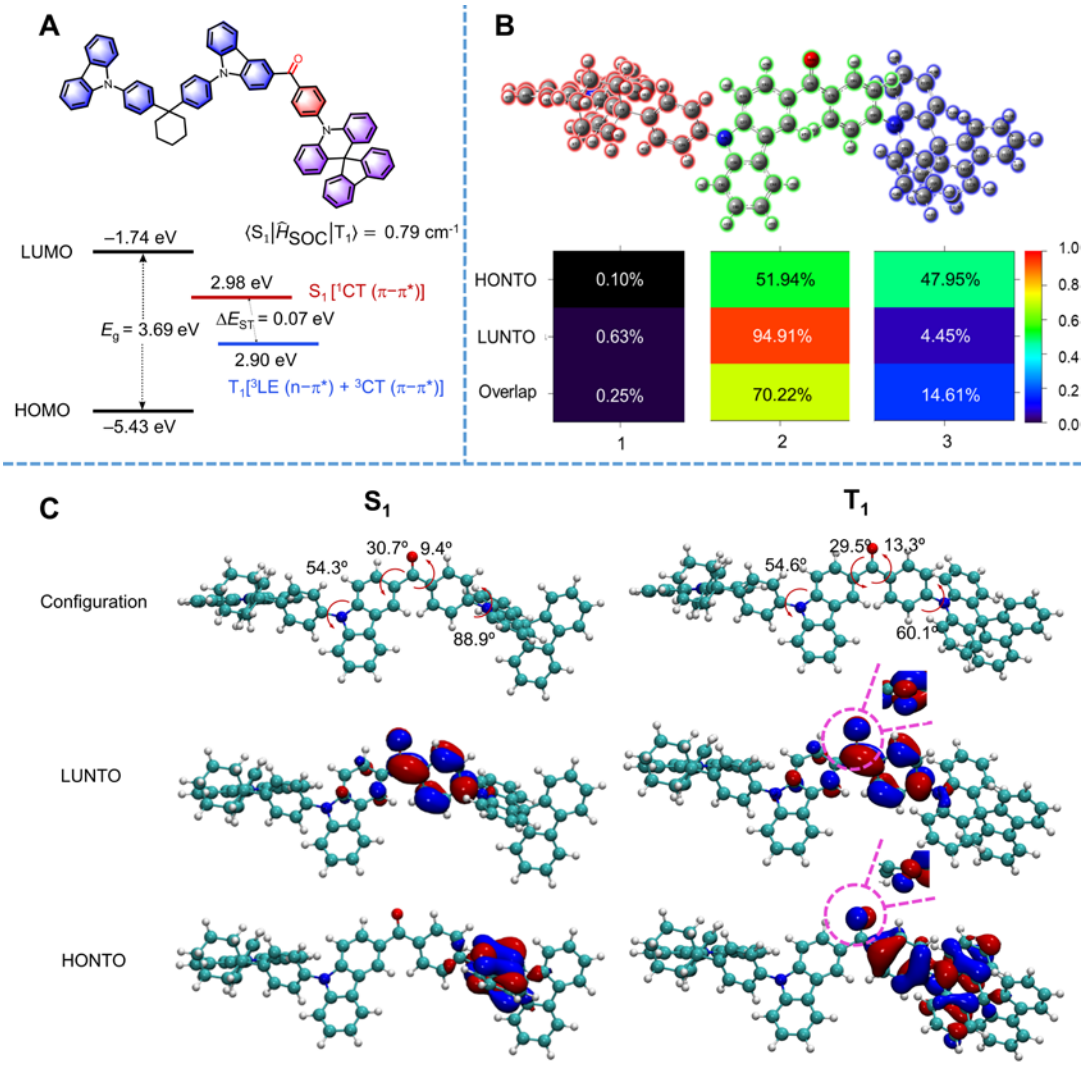

Figure 4. (A) Calculated HOMO and LUMO energy levels of the ground state, the energy level of S_1 and T_1 states and the SOC value between S_1 and T_1 states. (B) The distribution ratio and overlap ratio of the highest occupied natural transition orbital (HONTO) and the lowest unoccupied natural transition orbital (LUNTO) of T_1 state. The red, green and blue fragments of the molecule correspond to parts 1, 2 and 3, respectively. (C) The optimized geometrical structures and the natural transition orbital (NTO) analysis of S_1 and T_1 states. The encircled and enlarged parts indicate the feature of the n orbital.

According to the first-order perturbation theory:[15]

$$k_{RISC} \propto \left|\langle S_1|\hat{H}_{SOC}|T_1\rangle\right|^2 \exp\left[\frac{-\Delta E_{ST}}{k_B T}\right] \quad (1)$$

where $\langle S_1|\hat{H}_{SOC}|T_1\rangle$ is the SOC matrix element between S_1 and T_1 states, and ΔE_{ST} is the energy gap between S_1 and T_1 states. As for TADF emitters, small ΔE_{ST} and large SOC matrix element values are essential for fast RISC process. When it comes to ΔE_{ST} values, the common understanding is that the ΔE_{ST} is equal to twice the exchange energy, which is related to the overlap of transition orbitals. The smaller the overlap is, the smaller the exchange energy obtains. Meanwhile, on the basis of El-Sayed rule, the transition between LE-state and CT-state or between (π, π^*) and (n, π^*) is permitted and possesses a relatively lager SOC value, which is ascribed to the change of orbital angular momentum between these two states. Theoretically, with the S_1 state dominated by CT transition and the T_1 state governed by both LE and CT transitions, DCPC-BP-SFAC can have a much smaller ΔE_{ST} than the molecule with CT-type S_1 state and LE-type T_1 state, which always has a large SOC but a large ΔE_{ST}. And DCPC-BP-SFAC also obtains a larger SOC value than the molecule with CT-type S_1 state and CT-type T_1 state, which usually has a small ΔE_{ST} but a small SOC as well. The ΔE_{ST} and SOC values of DCPC-BP-SFAC are calculated to be 0.07 eV and 0.79 cm^{-1}, leading to fast RISC process, which is in good agreement with the experimental results.

2.2. Electroluminescence

2.2.1. Sky-Blue OLEDs Based on DCPC-BP-SFAC

The EL performance of DCPC-BP-SFAC is firstly evaluated in nondoped OLED (B1) with a configuration of ITO/HATCN (5 nm)/TAPC (50 nm)/TCTA (5 nm)/*m*CP (5 nm)/DCPC-BP-SFAC (20 nm)/PPF (5 nm)/TmPyPB (30 nm)/LiF (1 nm)/Al, where hexaazatriphenylenehexacabonitrile (HATCN) serves as hole injection layer, 1,1-bis[(di-4-tolylamino)phenyl]cyclohexane (TAPC) works as hole-transporting layer, tris[4-(carbazol-9-yl)phenyl]amine (TCTA) functions as hole buffer layer, 1,3-bis(carbazol-9-yl)benzene (*m*CP) and PPF serve as exciton blocking layer, and 1,3,5-tri(m-pyrid-3-yl-phenyl)benzene (TmPyPB) behaviors as electron transport layer (**Figure 5**A). The nondoped device B1 has a low turn-on voltage of 2.7 V and

radiates sky-blue light with a peak at 494 nm and Commission Internationale de I'Eclairage coordinates ($CIE_{x,y}$) of (0.199, 0.389). The maximum luminance, current efficiency (η_C), power efficiency (η_P) and η_{ext} are 36420 cd m^{-2}, 36.8 cd A^{-1}, 41.3 lm W^{-1} and 15.4%, respectively. It is noteworthy that the η_{ext} still maintains at 14.9% at 100 cd m^{-2} and 13.3% at 1000 cd m^{-2}, corresponding to 3.2% and 13.6% decrements in η_{ext} (Figure S3), respectively. The small efficiency roll-off is attributed to the fast RISC process, which alleviates the exciton concentration quenching dominated by short-range Dexter energy transfer at high voltages.[12,16]

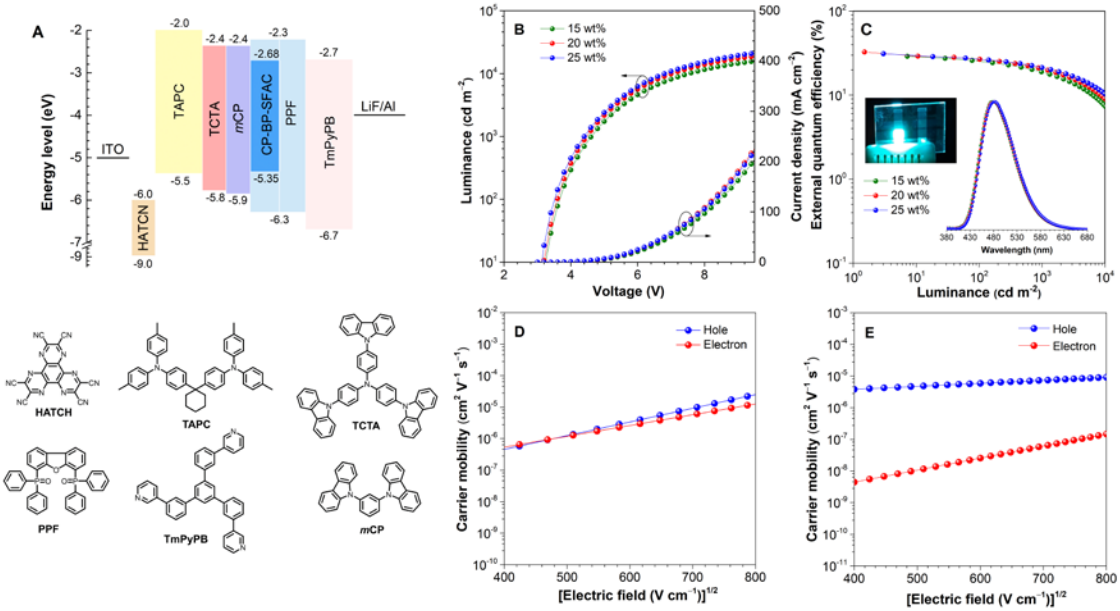

Figure 5. (A) Device architecture, energy diagram and functional layers for the OLEDs. (B) Luminance–voltage–current density and (C) external quantum efficiency–luminance of doped OLEDs. Inset in planes (C): EL spectra and photos of the doped devices with 20 wt% doping concentration at 4 V. Electric field-dependent carrier mobility of (D) neat film and (E) doped film of DCPC-BP-SFAC in single-carrier devices.

To further explore the EL performance of DCPC-BP-SFAC, doped OLEDs with a configuration of ITO/HATCN (5 nm)/TAPC (50 nm)/TCTA (5 nm)/*m*CP (5 nm)/*x* wt% DCPC-BP-SFAC: PPF (20 nm)/PPF (5 nm)/TmPyPB (30 nm)/LiF (1 nm)/Al are fabricated (*x* = 15, 20 and 25 for devices B2, B3 and B4, respectively). Benefiting from the matched HOMO and LUMO

energy levels of the function layers, the doped devices can be turned on at low voltages of ~3.0 V (Figure 5B). All the doped devices show sky-blue lights with EL peaks at around ~480 nm ($CIE_{x,y}$ = 0.160, 0.274). The EL efficiencies change little at different concentrations, indicating that DCPC-BP-SFAC can function efficiently at a wide range of doping concentrations (Figure 5C). The maximum η_{ext}, η_C and η_P values are 29.0%, 53.3 cd A^{-1} and 52.3 lm W^{-1} for B2, 32.6%, 61.2 cd A^{-1} and 64.1 lm W^{-1} for B3 and 31.1%, 59.8 cd A^{-1} and 62.6 lm W^{-1} for B4 (**Table 1**, Figure S4). Such outstanding η_{ext} values (29.0%–32.6%) demonstrate that these doped OLEDs are among the state-of-the-art sky-blue OLEDs in the literature.[1b,2c,9b,11a,17] Based on the data of $\Theta_{//}$, reflex index and thickness of the active layers, the η_{out} values are calculated to be 34.2% and 39.8% for the nondoped device (B1) and doped device (B3), respectively, which contribute greatly to the outstanding η_{ext} values. The efficiency roll-offs of the doped devices are somewhat higher than that of the nondoped device in spite of the close k_{RISC} values between neat and doped films. Concerning the dominating electron-transporting nature of PPF host, the unbalance of carrier mobility of the doped films might be accountable for the reduced η_{ext} at high voltages.

Table 1. EL performance of devices B1, B2, B3 and B4.[a)]

Device	V_{on} [V]	η_C [cd A^{-1}] Max/@100 cd m^{-2}/@1000 cd m^{-2}	η_P [lm W^{-1}] Max/@100 cd m^{-2}/@1000 cd m^{-2}	η_{ext} [%] Max/@100 cd m^{-2}/@1000 cd m^{-2}	L_{max} [cd m^{-2}]	CIE (x,y)	λ_{EL} [nm]
B1	2.7	36.8/35.9/31.9	41.3/38.4/29.0	15.4/14.9/13.3	36420	(0.199, 0.389)	494
B2	3.1	53.3/46.8/34.9	52.3/40.3/23.8	29.0/25.5/18.9	16630	(0.160, 0.266)	480
B3	3.0	61.2/50.3/38.8	64.1/44.0/27.3	32.6/26.8/20.7	19520	(0.160, 0.274)	482
B4	3.0	59.8/51.8/41.0	62.6/46.7/29.3	31.1/27.0/21.3	22350	(0.162, 0.284)	484

[a)]Abbreviations: V_{on} = turn-on voltage at 1 cd m^{-2}; $\eta_{ext}/\eta_C/\eta_P$ = external quantum efficiency/current efficiency/power efficiency; L_{max} = maximum luminance; CIE = Commission Internationale de l'Eclairage coordinates at 1000 cd m^{-2}; λ_{EL} = EL peak at 5 V.

2.2.2. Carrier Transport of DCPC-BP-SFAC

The carrier transport ability of the luminescent material plays an important role in determining the EL performance. The ideal condition is that the hole and electron mobilities are similar, or only slightly different, even at high voltages. Therefore, the hole and electron mobilities of the neat and doped films of DCPC-BP-SFAC are investigated by the space-charge limited current (SCLC) method. The hole-only devices with configurations of ITO/TAPC (10 nm)/DCPC-BP-SFAC or 20 wt% DCPC-BP-SFAC: PPF (80 nm)/TAPC (10 nm)/Al, and electron-only devices with configurations of ITO/TmPyPB (10 nm)/DCPC-BP-SFAC or 20 wt% DCPC-BP-SFAC: PPF (80 nm)/TmPyPB (10 nm)/LiF (1 nm)/Al are fabricated. The thin layers of TAPC and TmPyPB are used as buffer layers between emissive layer and the electrodes. The electric field-dependent carrier mobility is depicted in Figure 5D and 5E, and the carrier mobility is fitted by Mott-Gurney equation (2) and Poole–Frenkel formula (3):[18,19]

$$J = \frac{9}{8}\varepsilon_0\varepsilon_r\mu\frac{E^2}{L} = \frac{9}{8}\varepsilon_0\varepsilon_r\frac{V^2}{L^3}\mu_0\, exp\left(0.891\gamma\sqrt{\frac{V}{L}}\right) \quad (2)$$

$$\mu = \mu_0\, exp\left(\gamma\sqrt{E}\right) \quad (3)$$

where the ε_0 is the free-space permittivity (8.85×10^{-14} C V^{-1} cm^{-1}), ε_r stands for the relative dielectric constant (assumed to be 3.0 for organic semiconductors), E is the electric field, L is the thickness of the neat film and doped film, μ_0 is the zero-field mobility, and γ is the Poole-Frenkel factor.

It is obvious that the hole mobility (μ_h) and electron mobility (μ_e) of the neat film are quite close. At an electric field of 3.6×10^5 V cm^{-1}, the μ_h and μ_e values are 3.35×10^{-6} and 2.65×10^{-6} cm^2 V^{-1} s^{-1} for the neat film, indicating the balanced bipolar carrier transport of DCPC-BP-SFAC. However, for the doped film, the μ_h value (6.04×10^{-6} cm^2 V^{-1} s^{-1}) is about two orders of magnitude larger than the μ_e value (2.58×10^{-8} cm^2 V^{-1} s^{-1}), disclosing the unbalanced carrier transport. According to the μ_h and μ_e values of the doped film, it can be inferred that holes and electrons are injected into emissive layer mainly through DCPC-BP-SFAC and n-type host PPF, respectively.[20] The conjecture can be confirmed by the turn-on voltage, which is lower than the bandgap of PPF, but close to the energy level difference of DCPC-BP-SFAC's

HOMO and PPF's LUMO. Hence, the slow electron mobility of PPF play a negative effect on the exciton recombination at high voltages, accounting for EL efficiency decrease to some extent.[21]

2.2.3. Out-of-Phase Sensitized WOLEDs

All-fluorescence WOLEDs have drawn much attention as they are regarded as the promising candidates for next generation illumination.[22] The sensitization design strategy has been widely studied and successfully applied in the fabrication of WOLEDs. Comparing with conventional co-phase sensitizing system, out-of-phase sensitizing system can more effectively inhibit exciton loss caused by DET process, but still have much room for further optimization to improve EL performance by means of adopting more efficient emitter and host materials and device configuration engineering.[16,23] Owing to the balanced bipolar carrier transport characteristics and efficient EL performance of DCPC-BP-SFAC, it is employed as blue emitter and host material simultaneously to fabricate WOLEDs with an out-of-phase sensitizing configuration. To achieve high-quality white light with high color rendering index (CRI) values, a green TADF emitter, 3,6-bis(9,9-dimethylacridin-10-yl)xanthen-9-one (BDMAC-XT), an orange TADF emitter, 2,3,5,6-tetrakis(3,6-di-(*tert*-butyl)carbazol-9-yl)-1,4-dicyanobenzene (4CzTPNBu), and a red conventional fluorescence emitter, 5,10,15,20-tetraphenylbisbenz[5,6]indeno[1,2,3-cd:1′,2′,3′-lm]perylene (DBP) are selected to work with sky-blue DCP-BP-DPAC (**Figure 6**A). It is envisioned that efficient FET can occur between DCPC-BP-SFAC and other emitters doped in DCPC-BP-SFAC because of the overlaps of the emission and absorption spectra (Figure S5). The interlayer is removed to simplify the device manufacturing process. The removal of interlayer in this work is an important advancement in comparison with the previously reported out-of-phase sensitizing configuration of WOLEDs.[16] The device configuration is ITO/HATCN (5 nm)/TAPC (50 nm)/1 wt% DBP: TCTA (5 nm)/2 wt% 4CzTPNBu: 30 wt% BDMAC-XT: host (5 nm)/20 wt% DCPC-BP-SFAC: PPF (8 nm)/PPF (5

nm)/TmPyPB (30 nm)/LiF (1 nm)/Al, in which the host materials are DCPC-BP-SFAC, 3,3'-di(9H-carbazol-9-yl)-1,1'-biphenyl (mCBP), TmPyPB and 2,6-di(9H-carbazol-9-yl)pyridine (PYD-2Cz) for W1, W2, W3 and W4, respectively.

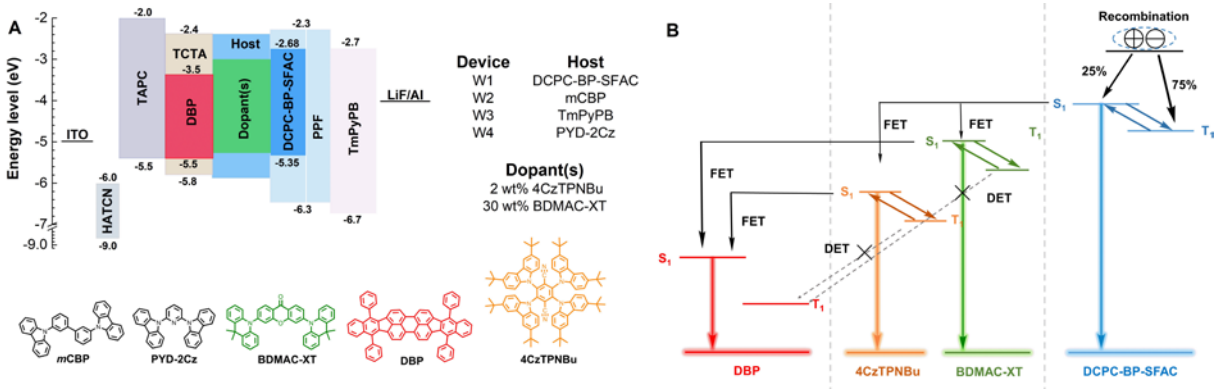

Figure 6. (A) Device architecture, energy diagram and functional layers for the WOLEDs. (B) The schematical illustration of energy transfer process in W1.

The obtained WOLEDs show stable EL spectra even at high luminance of 20000 cd m^{-2}, indicative of the ultra-stable exciton allocation among these emitters. Among them, W1 exhibits superior EL performance with a small turn-on voltage of only 2.5 V and maximum EL efficiencies of 53.5 cd A^{-1}, 64.6 lm W^{-1} and 21.7% (**Figure 7**, Figure S6). Moreover, the CRI value of W1 reaches a peak of 72 and maintains at 70 at the luminance of 1000 cd m^{-2} (Table 2). For comparison, the device performances of W2 and W3 employing p-type host mCBP and n-type host TmPyPB, respectively, are investigated. W2 attains high EL efficiencies of 58.5 cd A^{-1},

Table 2. EL performance of WOLEDs.[a)]

De-vice	V_{on} [V]	η_C [cd A^{-1}] Max/@1000 cd m^{-2}	η_P [lm W^{-1}] Max/@1000 cd m^{-2}	η_{ext} [%] Max/@1000 cd m^{-2}	L_{max} [cd m^{-2}]	CIE (x,y)	CRI Max/1000 cd m^{-2}
W1	2.5	53.5/39.4	64.6/35.4	21.7/15.3	28720	(0.350,0.466)	72/70
W2	2.7	58.5/37.0	65.7/33.2	22.4/15.0	25930	(0.257,0.419)	59/52
W3	2.6	56.4/40.4	63.2/36.3	20.3/14.8	21660	(0.319,0.480)	60/56
W4	2.7	49.8/29.3	55.8/26.3	19.5/12.0	23400	(0.297,0.424)	69/66
W5	2.6	48.1/28.1	58.1/26.5	21.6/12.2	23150	(0.465,0.462)	84/76

[a)] V_{on} = turn-on voltage at 1 cd m^{-2}; $\eta_{ext}/\eta_C/\eta_P$ = external quantum efficiency/current efficiency/power efficiency; L_{max} = maximum luminance; CIE = Commission Internationale de l'Eclairage coordinates at 1000 cd m^{-2}; CRI = color rendering index.

65.7 lm W^{-1} and 22.4%. But the color quality is decreased, with a CRI of only 59 because of the larger weighting at blue emissive part as shown in EL spectra. The exciton recombination zone is concentrated at the blue-emitting layer, due to the p-type characteristic of mCBP. W3 is slightly less efficient than W2, with EL efficiencies of 56.4 cd A^{-1}, 63.2 lm W^{-1} and 20.3%, and has a similar CRI of 60 to that of W2. The weighting of red emissive part is slightly increased as depicted in Figure 7D, which is probably caused by the n-type characteristic of TmPyPB. W4 adopting the bipolar host PYD-2Cz provides good color quality with a CRI of 69, which is comparable to that of W1, but its EL efficiencies (49.8 cd A^{-1}, 55.8 lm W^{-1} and 19.5%) are slightly lowered. The turn-on voltage of W4 is higher than W1, mainly due to the larger energy gap of PYD-2Cz. The larger energy gap also raises the threshold of carrier injections, which is probably responsible for the efficiency reduce of W4. In addition to the bipolar carrier transport and the small energy gap, the good EL performance of DCPC-BP-SFAC also ensures efficient host-guest FET and reduced annihilation of triplet excitons to a large extent.

To further confirm the balanced distribution of exciton recombination zone in W1, an ultrathin red DBP layer (0.05 nm) is placed at different positions of the green-orange emitting layer of W1 without DBP dopant in TCTA, and the corresponding device configuration is presented in Figure S7. The red detection layer DBP is inserted at 1, 2, 3 and 4 nm from the left of

the orange-green emitting layer. As shown in Figure S8, the spectra are almost invariant with the detection layer at different positions, indicating that the exciton allocation inside the green-orange emitting layer with DCPC-BP-SFAC host is balanced even at high voltages, which contributes to efficient FET process and better color quality.

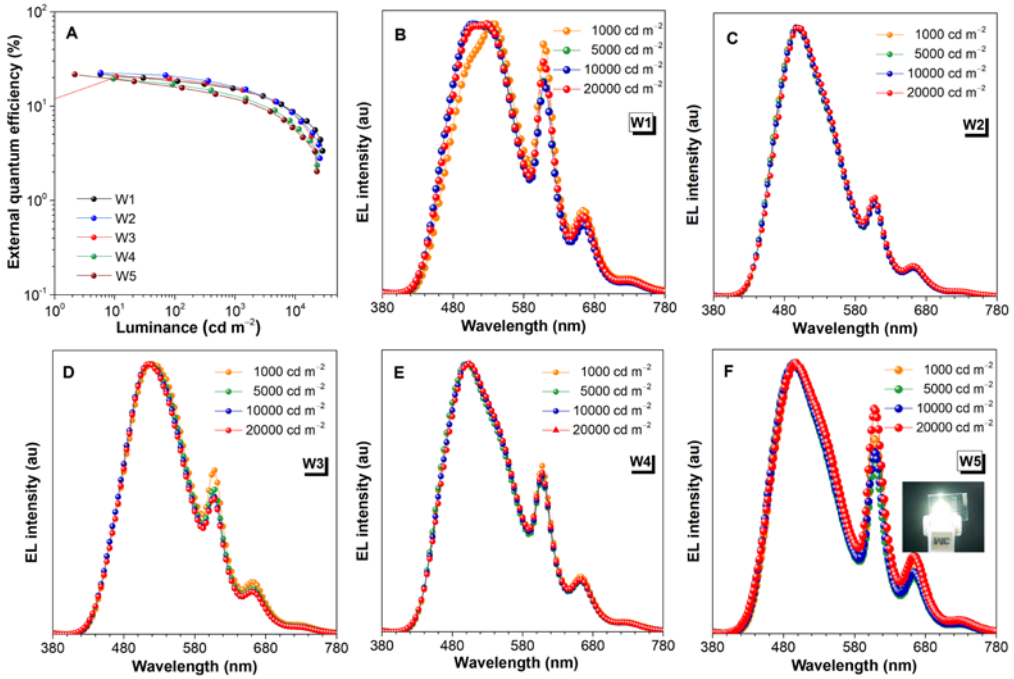

Figure 7. (A) External quantum efficiency–luminance. EL spectra of (B) W1, (C) W2, (D) W3, (E) W4 and (F) W5 at 1000, 5000, 10000 and 20000 cd m^{-2}.

For the white-light illumination, the higher the CRI, the better the visual experience. To increase the CRI value, the WOLED structure is further optimized based on W1 with the configuration of ITO/HATCN (5 nm)/TAPC (50 nm)/1 wt% DBP: TCTA (10 nm)/2 wt% 4CzTPNBu: 30 wt% BDAMC-XT: DCPC-BP-SFAC (3 nm)/20 wt% DCPC-BP-SFAC: PPF (7 nm)/PPF (5 nm)/TmPyPB (30 nm)/LiF (1 nm)/Al (W5). Comparing with W1, W5 possesses a thicker red emitting layer and a thinner green-orange emitting layer as well as a thinner sky-blue emitting layer to adjust the proportion of each color. By this modulation, W5 radiates warm-white light with a CRI as high as 84, which is improved apparently relative to that of W1 (CRI = 72), validating that the strategy adopted is feasible. Meanwhile, W5 also affords stable

EL spectra and good EL performances with a low turn-on voltage of 2.6 V and maximum EL efficiencies of 48.1 cd A^{-1}, 58.1 lm W^{-1} and 21.6% (Table 2, Figure 7A, 7F and FigureS6).

3. Conclusion

In conclusion, a novel luminogen (DCPC-BP-SFAC) consisting of a carbonyl acceptor and SFAC and DCPC donors is successfully designed and synthesized. DCPC-BP-SFAC enjoys excellent thermal and electrochemical stabilities and balanced bipolar carrier transport ability. It exhibits strong sky-blue delayed fluorescence with high Φ_{PL} values of up to 90% and fast RISC process. The small ΔE_{ST} and large SOC values of DCPC-BP-SFAC originating from the S_1 state dominated by CT transition and the T_1 state governed by both LE and CT transitions account for the efficient delayed fluorescence. Moreover, due to the presence of spiro-structured SFAC, DCPC-BP-SFAC prefers horizontal orientation of emitting dipole, rendering a large $\Theta_{//}$ of 85% and thus a high η_{out} of 39.8%. High-performance sky-blue OLEDs are achieved based on DCPC-BP-SFAC, providing outstanding maximum η_{ext} values of up to 32.6% at an EL peak at 482 nm. And efficient all-fluorescence WOLEDs with an out-of-phase sensitizing configuration in absence of interlayers are fabricated by using DCPC-BP-SFAC as both blue emitter and host material, radiating stable warm-white light with a high CRI of 84, and furnishing excellent EL performance of a small turn-on voltage of 2.6 V, and maximum EL efficiencies of 48.1 cd A^{-1}, 58.1 lm W^{-1} and 21.6%. The superior comprehensive EL performance resulting from fast RISC process, balanced carrier transport and preferable horizontal orientation makes DCPC-BP-SFAC a promising candidate for OLEDs.

Supporting Information

Supporting Information is available from the Wiley Online Library or from the author.

Acknowledgements

This study was financially supported by the National Natural Science Foundation of China (21788102), the Natural Science Foundation of Guangdong Province (2019B030301003) and the Innovation and Technology Commission (ITC-CNERC14SC01).

Received: ((will be filled in by the editorial staff))
Revised: ((will be filled in by the editorial staff))
Published online: ((will be filled in by the editorial staff))

References

[1] a) C. W. Tang, S. A. VanSlyke, *Appl. Phys. Lett.* **1987**, *51*, 913; b) D. H. Ahn, S. W. Kim, H. Lee, I. J. Ko, D. Karthik, J. Y. Lee, J. H. Kwon, *Nat. Photon.* **2019**, *13*, 540; c) S. Hirata, Y. Sakai, K. Masui, H. Tanaka, S. Y. Lee, H. Nomura, N. Nakamura, M. Yasumatsu, H. Nakanotani, Q. Zhang, K. Shizu, H. Miyazaki, C. Adachi, *Nat. Mater.* **2015**, *14*, 330.

[2] a) C. Mayr, S. Lee, T. Schmidt, T. Yasuda, C. Adachi, W. Brütting, *Adv. Funct. Mater.* **2014**, *24*, 5232; b) J. Kim, T. Yasuda, Y. Yang, C. Adachi, *Adv. Mater.* **2013**, *25*, 2666; c) B. Sim, C.-K. Moon, K.-H. Kim, J.-J. Kim, *ACS Appl. Mater. Interfaces* **2016**, *8*, 33010.

[3] a) D. Zhang, J. Qiao, D. Zhang, L. Duan, *Adv. Mater.* **2017**, *29*, 1702847; b) K. Tuong Ly, R.-W. Chen-Cheng, H.-W. Lin, Y.-J. Shiau, S.-H. Liu, P.-T. Chou, C.-S. Tsao, Y.-C. Huang, Y. Chi, *Nat. Photon.* **2016**, *11*, 63; c) X. Tang, L. S. Cui, H. C. Li, A. J. Gillett, F. Auras, Y. K. Qu, C. Zhong, S. T. E. Jones, Z. Q. Jiang, R. H. Friend, L. S. Liao, *Nat. Mater.* **2020**, *19*, 1332.

[4] a) H. Sasabe, H. Nakanishi, Y. Watanabe, S. Yano, M. Hirasawa, Y. J. Pu, J. Kido, *Adv. Funct. Mater.* **2013**, *23*, 5550; b) M. A. Baldo, D. F. O'Brien, Y. You, A. Shoustikov, S. Sibley, M. E. Thompson, S. R. Forrest, *Nature* **1998**, *395*, 151; c) C. Adachi, M. A. Baldo, M. E. Thompson, S. R. Forrest, *J. Appl. Phys.* **2001**, *90*, 5048.

[5] a) P. K. Samanta, D. Kim, V. Coropceanu, J. L. Bredas, *J. Am. Chem. Soc.* **2017,** *139*, 4042; b) J. J. Guo, J. Z. Fan, L. L. Lin, J. J. Zeng, H. Liu, C. K. Wang, Z. J. Zhao, B. Z. Tang, *Adv. Sci.* **2019,** *6*, 9; c) I. S. Park, K. Matsuo, N. Aizawa, T. Yasuda, *Adv. Funct. Mater.* **2018**, *28*, 1802031.

[6] a) J. Rao, L. Yang, X. Li, L. Zhao, S. Wang, J. Ding, L. Wang, *Angew. Chem. Int. Ed.* **2020**, *59*, 17903; b) M. Y. Wong, E. Zysman-Colman, *Adv. Mater.* **2017**, *29*, 1605444; c) M. Godumala, J. Hwang, H. Kang, J.-E. Jeong, A. K. Harit, M. J. Cho, H. Y. Woo, S. Park, D. H. Choi, *ACS Appl. Mater. Interfaces* **2020**, *12*, 35300.

[7] a) J. Zeng, J. Guo, H. Liu, Z. Zhao, B. Z. Tang, *Adv. Funct. Mater.* **2020**, *30*, 2000019; b) Zhang, X. Song, M. Cai, H. Kaji, L. Duan, *Adv. Mater.* **2018**, *30*, 1705406; c) J. Chen, J. Zeng, X. Zhu, J. Guo, Z. Zhao, B. Z. Tang, *CCS Chem.* **2021**, *3*, 230.

[8] Z. Wang, M. Helander, J. Qiu, D. Puzzo, M. Greiner, Z. Liu, Z. Lu, *Appl. Phys. Lett.* **2011**, *98*, 39.

[9] a) H. Liu, J. Zeng, J. Guo, H. Nie, Z. Zhao, B. Z. Tang, *Angew. Chem. Int. Ed.* **2018**, *57*, 9290; b) W. Li, B. Li, X. Cai, L. Gan, Z. Xu, W. Li, K. Liu, D. Chen, S.-J. Su, *Angew. Chem. Int. Ed.* **2019**, *58*, 11301; c) Y. Fu, H. Liu, X. Zhu, J. Zeng, Z. Zhao, B. Z. Tang, *J. Mater. Chem. C* **2020**, *8*, 9549.

[10] a) I. S. Park, H. Seo, H. Tachibana, J. U. Kim, J. Zhang, S. M. Son, T. Yasuda, *ACS Appl. Mater. Interfaces* **2017**, *9*, 2693; b) D. W. Lee, J. Hwang, H. J. Kim, H. Lee, J. M. Ha, H. Y. Woo, S. Park, M. J. Cho, D. H. Choi, *ACS Appl. Mater. Interfaces* **2021**, 10.1021/acsami.1c14098.

[11] a) T.-A. Lin, T. Chatterjee, W.-L. Tsai, W.-K. Lee, M.-J. Wu, M. Jiao, K.-C. Pan, C.-L. Yi, C.-L. Chung, K.-T. Wong, C.-C. Wu, *Adv. Mater.* **2016**, *28*, 6976; b) X. Gong, P. Li, Y.-H. Huang, C.-Y. Wang, C.-H. Lu, W.-K. Lee, C. Zhong, Z. Chen, W. Ning, C.-C. Wu, S. Gong, C. Yang, *Adv. Funct. Mater.* **2020**, *30*, 1908839; c) H. Lim, H. J. Cheon, S.-J. Woo, S.-K. Kwon, Y.-H. Kim, J.-J. Kim, *Adv. Mater.* **2020**, *32*, 2004083.

[12] a) J. Guo, X.-L. Li, H. Nie, W. Luo, S. Gan, S. Hu, R. Hu, A. Qin, Z. Zhao, S.-J. Su, B. Z. Tang, *Adv. Funct. Mater.* **2017**, *27*, 1606458; b) J. Huang, H. Nie, J. Zeng, Z. Zhuang, S. Gan, Y. Cai, J. Guo, S.-J. Su, Z. Zhao, B. Z. Tang, *Angew. Chem., Int. Ed.* **2017**, *56*, 12971.

[13] C. Han, G. Xie, J. Li, Z. Zhang, H. Xu, Z. Deng, Y. Zhao, P. Yan, S. Liu, *Chem. Eur. J.* **2011**, *17*, 8974.

[14] a) Q. Zhang, H. Kuwabara, W. J. Potscavage Jr., S. Huang, Y. Hatae, T. Shibata, C. Adachi, *J. Am. Chem. Soc*. **2014**, *136*, 18070; b) L.-S. Cui, A. J. Gillett, S.-F. Zhang, H. Ye, Y. Liu, X.-K. Chen, Z.-S. Lin, E. W. Evans, W. K. Myers, T. K. Ronson, H. Nakanotani, S. Reineke, J.-L. Bredas, C. Adachi, R. H. Friend, *Nat. Photonics* **2020,** *14*, 636.

[15] a) P. K. Samanta, D. Kim, V. Coropceanu, J. L. Brédas, *J. Am. Chem. Soc*. **2017**, *139*, 4042. b) D. Beljonne, Z. Shuai, G. Pourtois, J. L. Brédas, *J. Phys. Chem. A* **2001**, *105*, 3899.

[16] H. Liu, J. Chen, Y. Fu, Z. Zhao, B. Z. Tang, *Adv. Funct. Mater.* **2021**, *31*, 2103273.

[17] a) W. Li, M. Li, W. Li, Z. Xu, L. Gan, K. Liu, N. Zheng, C. Ning, D. Chen, Y.-C. Wu, S.-J. Su, *ACS Appl. Mater. Interfaces* **2021**, *13*, 5302; b) J. Jayakumar, T. L. Wu, M. J. Huang, P. Y. Huang, T. Y. Chou, H. W. Lin, C. H. Cheng, *ACS Appl. Mater. Interfaces* **2019**, *11*, 21042; c) C. Li, C. Duan, C. Han, H. Xu, *Adv. Mater.* **2018**, *30*, 1804228; d) M. Liu, R. Komatsu, X. Cai, K. Hotta, S. Sato, K. Liu, D. Chen, Y. Kato, H. Sasabe, S. Ohisa, Y. Suzuri, D. Yokoyama, S.-J. Su, J. Kido, *Chem. Mater.* **2017**, *29*, 8630.

[18] Z. S. An, J. S. Yu, S. C. Jones, S. Barlow, S. Yoo, B. Domercq, P. Prins, L. D. A. Siebbeles, B. Kippelen, S. R. Marder, *Adv. Mater.* **2015**, *17*, 2580.

[19] G. Lin, H. Peng, L. Chen, H. Nie, W. Luo, Y. Li, S. Chen, R. Hu, A. Qin, Z. Zhao, B. Z. Tang, *ACS Appl. Mater. Interfaces* **2016**, *8*, 16799.

[20] H. Lim, H. J. Cheon, S.-J. Woo, S.-K. Kwon, Y.-H. Kim, J.-J. Kim, *Adv. Mater.* **2020**, *32*, 2004083

[21] a) L. Su, F. Cao, C. Cheng, T. Tsuboi, Y. Zhu, C. Deng, X. Zheng, D. Wang, Z. Liu, Q. Zhang, *ACS Appl. Mater. Interfaces* **2020**, *12*, 31706; b) N. Lin, J. Qiao, L. Duan, H. Li, L. Wang, Y. Qiu, *J. Phys. Chem. C* **2012**, *116*, 19451.

[22] a) X.-L. Li, G. Xie, M. Liu, D. Chen, X. Cai, J. Peng, Y. Cao, S.-J. Su, *Adv. Mater*. **2016**, *28*, 4614; b) Z. Wu, Y. Liu, L. Yu, C. Zhao, D. Yang, X. Qiao, J. Chen, C. Yang, H. Kleemann,

K. Leo, D. Ma, Nat. Commun. 2019, 10, 2380; c) Y. Liu, X. Wei, Z. Li, J. Liu, R. Wang, X. Hu, P. Wang, T. Qi, Y. Wang, *Adv. Opt. Mater.* **2018**, *6*, 1800978.

[23] a) D. Zhang, X. Song, H. Li, M. Cai, Z. Bin, T. Huang, L. Duan, *Adv. Mater.* **2018**, *30*, 1707590; b) S. H. Han, J. Y. Lee, *J. Mater. Chem. C* **2018**, *6*, 1504.

Table of Contents

A tailor-made sky-blue delayed fluorescence luminogen with strong photoluminescence, fast reverse intersystem crossing, balanced carrier transport, horizontal dipole orientation and large light out-coupling efficiency is explored, which furnishes outstanding external quantum efficiencies of 32.6% as emitter in sky-blue OLEDs and 21.7% as emitter and host simultaneously in all-fluorescence white OLEDs.